A Methodology for Characterizing Weldment Fracture Behavior

Criteria to predict failure in high-strength steel weldments containing incomplete penetration are established

BY E. P. COX

ABSTRACT. Collapse stresses of flawed structural steel weldments were predicted by a two failure criteria model based on plasticity limit load theory and linear elastic fracture mechanics. This model, first applied to wrought steels covering wide ranges of strengths and toughnesses, was subsequently modified for application to the particular case of structural steel weldments. Failure commenced whenever the flawed component reached either the fracture toughness (FT) failure criterion or the plasticity limit load (LL) failure criterion. In all instances, the controlling failure criterion depended on tensile strength, fracture toughness, section size and, specifically, on the magnitude of $\frac{Kc}{Su\sqrt{W}}$. In general, low values of $\frac{Kc}{Su\sqrt{W}}$ cause FT controlled fractures, and high values of $\frac{Kc}{Su\sqrt{W}}$ cause LL controlled fractures. An *a priori* determination of the controlling failure criterion was shown to be feasible.

Interactions of the various weldment zones, *e.g.*, base metal, heat affected zones, weld metal passes, etc., often redistributed the stresses and strains in flawed welds. Depending on the extent of weld metal strength overmatching, a third failure criterion and two transition flaw sizes dictated weldment fracture behavior. Based on experimental results, a method was devised to determine the controlling fracture criterion for a wide variety of steel weldments. In addition, the effects of local and gross section plasticity were considered, as well as how the presence of stable tearing could cause a change from one failure criterion to another.

E. P. COX is a Staff Engineer with Materials Analysis, Inc., Dallas, Tex.

Introduction

With the advent of fracture mechanics, a total disregard has sometimes developed as to when fracture mechanics is an appropriate tool for predicting critical crack size or fracture stress in tough, structural steels, and when it is not. Most disconcerting is that a pure fracture mechanics approach can predict an unrealistically large critical crack size and failure load beyond the tensile strength of the component. Such misapplications have actually occurred in several companies.

The intent of this paper is to prevent catastrophic misuse of fracture mechanics, particularly when it is promulgated as the panacea for determining accept/reject criteria for flawed components. To accomplish its purpose, the paper examines experimental data originally developed by the author and Professor F. V. Lawrence, Jr. (Refs. 11, 12, 22) and does so to develop an analytical scheme in order to derive *a priori* predictive techniques.

Examination of Planar Discontinuities

The mechanical properties of welded joints can be significantly reduced by the presence of internal discontinuities, such as: porosity, entrapped slag, incomplete sidewall fusion, inadequate joint penetration, and cracks (Refs. 1–7). Planar discontinuities, notably cracks and incomplete joint penetration, are particularly deleterious. Such planar discontinuities, upon reaching a critical size, can reduce weld joint ductility and promote brittle fracture.

Tilted and/or intermittent flaws are treated in the same manner as perpendicular, planar cracks. More specifically, the applicable fracture mechanics analysis is determined (or selected from published solutions) along with the appropriate limit load analysis. In some instances, the limit load analysis and/or fracture mechanics analysis cannot be determined exactly, and one has then to rely on an engineering judgment as to whether an upper bound or lower bound analysis best represents the problem.

Depending on the size and geometry of a discontinuity relative to that of the weldment and the fracture toughness of the volume of material containing the discontinuity, a fracture mechanics approach can sometimes be used to characterize fracture behavior. Linear elastic fracture mechanics (LEFM) can often be used for heavy sections fabricated from low toughness materials. The ductile materials commonly used in engineering applications usually fracture at loads beyond the yield strength and then only after extensive plastic deformation has occurred. The fracture loads of these high toughness materials often cannot be successfully predicted by LEFM, particularly for the thicknesses in common usage.

Attempts to characterize ductile, post-yield fractures using elastic-plastic fracture mechanics analyses have met with varying degrees of success. One of the most promising of the elastic-plastic analyses is the J-integral proposed by Rice (Ref. 8). Experimental results have demonstrated that the J-integral can be used

KEY WORDS

Steel Weld Fracture
Structural Steel Weld
Gas Metal Arc Welding
Planar Discontinuity
Ductile Fracture
Fracture Mechanics
Two Failure Criteria
Fracture Toughness
LEFM Equations
ASTM A514 GrF Steel

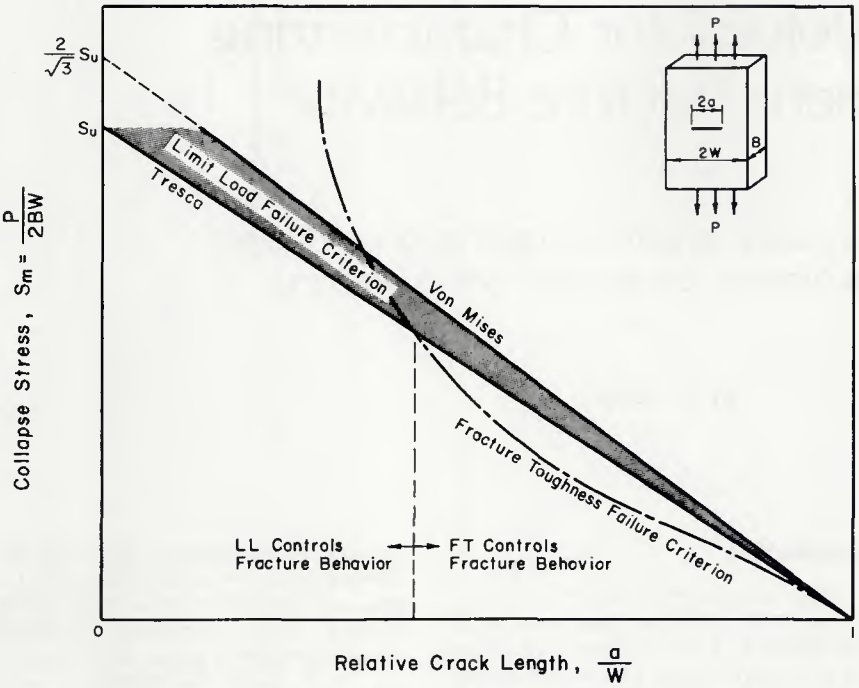

Fig. 1—Illustration of the two failure criteria model for a center-crack tension specimen

to measure the plane-strain fracture toughness of ductile materials undergoing elastic-plastic deformation (Refs. 9, 10), and the J-integral, therefore, may provide a single factor for characterizing postyield fracture.

This and other recent investigations by the author (Refs. 4, 11–13) and Dowling and Townley (Ref. 14) have shown that ductile fracture may also be characterized using a two criteria approach based on fracture mechanics and plastic limit load analyses. The fracture toughness failure criterion describes a fracture which will occur whenever the crack tip stress intensity exceeds the material's fracture toughness. The limit load failure criterion describes a fracture (or collapse) which will occur when the load on the uncracked ligament reaches the limit load of the body. The limit load is the maximum load that a body can sustain without undergoing unlimited plastic deformation (Refs. 15, 16). The maximum (collapse) load or stress for a body is the lower value predicted by the two failure criteria.

The Two Failure Criteria Model for Homogeneous Materials

An example of the two failure criteria model is given below for a center-cracked-tension specimen (CCT). The gross section stress at collapse (S_m) for the CCT specimen geometry is given by (Ref. 17):

$$S_m = \frac{P_m}{2BW} = 2\tau_o(1 - \frac{a}{W}) \qquad (1)$$

where: p_m is collapse load, B is specimen thickness, 2W is specimen width, and 2a is crack width, which becomes a failure criterion when shear flow stress at fracture (τ_o) is replaced by either the von Mises or Tresca yield criterion. That is, the collapse stress predicted using the von Mises yield criterion is:

$$S_m^M = \frac{2}{\sqrt{3}} S_u (1 - \frac{a}{W}) \qquad (2)$$

and similarly, the collapse stress using the Tresca yield criterion is:

$$S_m^T = S_u(1 - \frac{a}{W}) \qquad (3)$$

The curves corresponding to the von Mises and Tresca values of collapse stress are shown as solid lines in Fig. 1. The region between these lines is labeled "Limit Load Failure Criterion" to illustrate the range in collapse stress predicted by the LL failure criterion. Most test data fall in the shaded region, because structural materials generally obey neither the von Mises nor Tresca yield criterion.

The collapse stress curve predicted by the fracture toughness failure criterion for the center-crack specimen geometry (S_m^K) is given by the equation:

$$S_m^K = \frac{K_c}{(\pi a)^{1/2} (\sec\frac{\pi a}{2W})^{1/2}} \qquad (4)$$

where: K_c is fracture toughness measured either by ASTM E399 (Ref. 18) test procedures (K_{Ic}) or determined from a J-integral test (J_{Ic}) (Ref. 19). This curve in Fig. 1 is labeled "Fracture Toughness Failure Criterion" and is shown crossing the region labeled "Limit Load Failure Criterion." The value of S_m^K is dependent on K_c, a, and W, whereas S_m^M and S_m^T are dependent on S_u, a, and W. Consequently, as S_u, W, and K_c change, the value of S_m also changes. In many instances, there is no intersection between the LL and FT failure criteria, hence only one failure criterion prevails. For the case where an intersection does occur, such as is shown in Fig. 1, the collapse stress will be that of the failure criterion which operates at the lower stress. In Fig. 1, the LL failure criterion controls fracture at smaller values of a/W and the FT failure criterion controls fracture at larger values of a/W.

A transition from one failure criterion to another should occur (approximately) whenever $S_m^T = S_m^K$; but, this will occur only at certain combinations of specimen dimensions, tensile strength, fracture toughness and crack length—Fig. 1. The crack length for this transition can be determined by equating the LL and FT collapse loads given by Equations 2–4:

$$S_m^M \text{ or } S_m^T = S_M^k \qquad (5)$$

which, for the CCT geometry and the Tresca yield criterion, becomes:

$$S_u (1 - \frac{a}{W}) = \frac{K_c}{(\pi a \sec\frac{\pi a}{2W})^{1/2}} \qquad (6)$$

This equation can be rearranged in terms of a/W to yield the following equation:

$$\frac{K_c}{S_u\sqrt{W}} = (1 - \frac{a}{W})(\frac{\pi a}{W} \sec\frac{\pi a}{2W})^{1/2} \qquad (7)$$

The right-hand side of Equation 7 is multiplied by $2/\sqrt{3}$ when the von Mises yield criterion is desired.

The quantity $K_c/S_u\sqrt{W}$ relates the strength, fracture toughness and section size to the controlling failure criterion. This quantity is plotted versus a/W in Fig. 2 for the CCT specimen geometry and in Fig. 3 for the three-point bend specimen. When K_c is low and S_u is high, which corresponds to a low value of $K_c/S_u\sqrt{W}$, the fracture toughness failure criterion dominates the fracture behavior. Increasing K_c and decreasing S_u increases the value of $K_c/S_u\sqrt{W}$ into the limit load region. Crack length also affects which failure criterion controls fracture. In Fig. 2, for instance, at $K_c/S_u\sqrt{W} = 0.6$, the controlling failure criterion changes from LL to FT at an a/W of approximately 0.1 and from FT back to LL at an a/W of approximately 0.85.

A second illustration of the two failure criteria is given for the compact specimen geometry shown in Fig. 4. Since an exact limit load solution is not available, upper

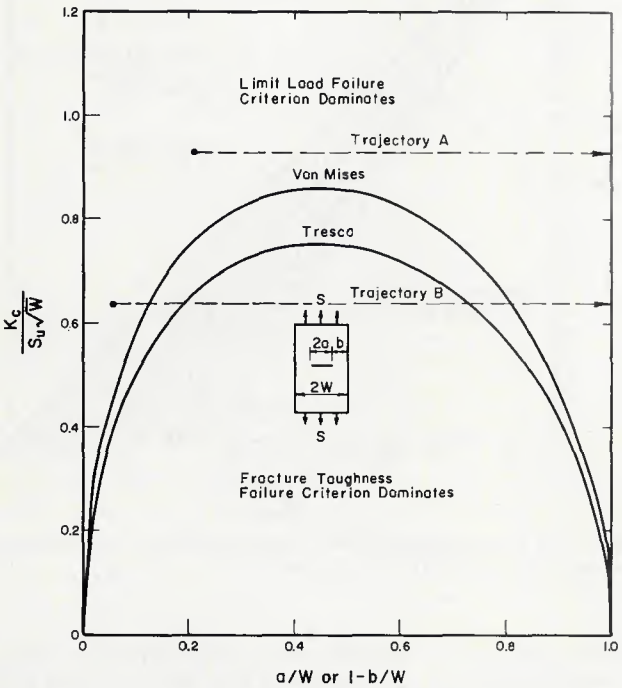

Fig. 2—Limit load and fracture toughness failure criteria controlled fracture regions for the center-crack tension specimen

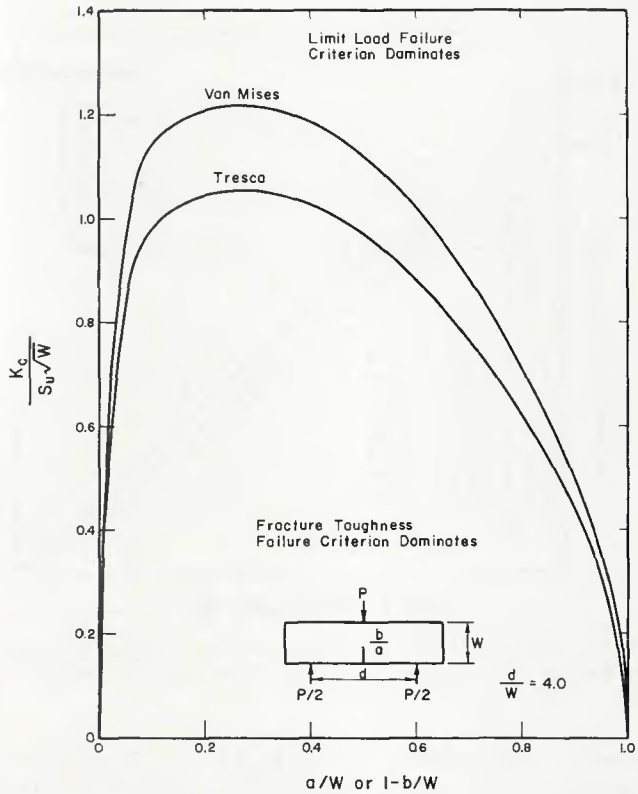

Fig. 3—Limit load and fracture toughness failure criteria controlled fracture regions for the three-point bend specimen

(Ref. 20) and lower (Ref. 21) bound solutions are shown using both the von Mises and Tresca yield criteria. To be conservative, the lower bound LL solution is utilized. The lower bound LL expression is:

$$P_L = \{\sqrt{2}\,[1+\frac{a}{W}]^{1/2} - [1+\frac{a}{W}]\}\,(2\tau_o)\,BW \qquad (8)$$

which, when rearranged and when the von Mises yield criterion is inserted for the flow stress, results in a collapse load given by:

$$\frac{P_L}{BW} = \{\sqrt{2}\,[1+\frac{a}{W}]^{1/2} - [1+\frac{a}{W}]\}\,\frac{2}{\sqrt{3}}S_u \qquad (9)$$

Using the Tresca yield criterion, the collapse load is:

$$\frac{P_L}{BW} = \{\sqrt{2}\,[1+\frac{a}{W}]^{1/2} - [1+\frac{a}{W}]\}\,S_u \qquad (10)$$

When the FT failure criterion is used to predict the collapse load in a compact specimen, the collapse load is given by:

$$\frac{P_K}{BW} = \frac{K_{Ic}}{Y\sqrt{W}} \qquad (11)$$

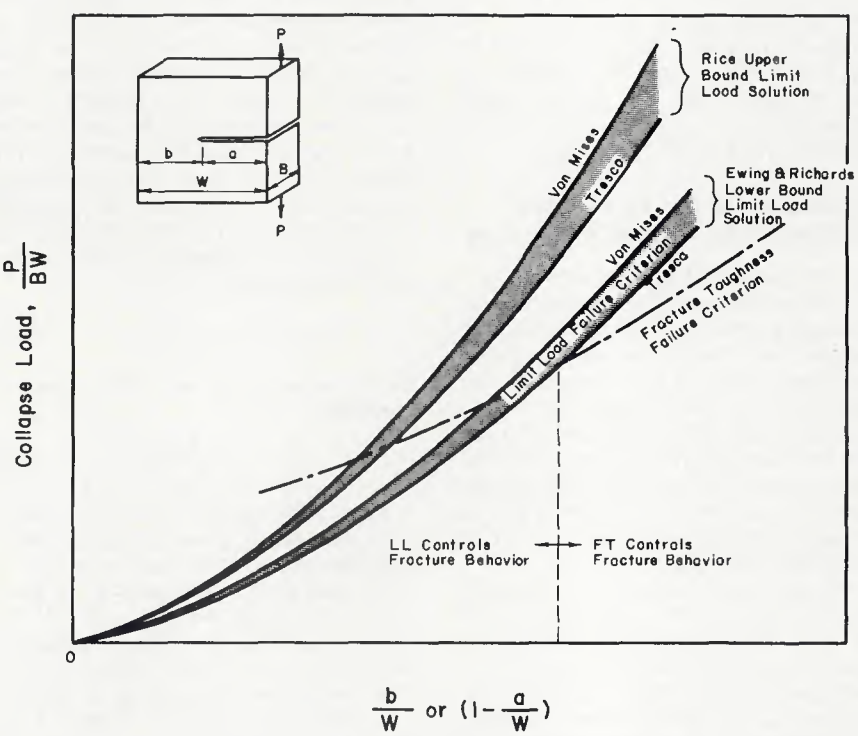

Fig. 4—Illustration of the two failure criteria model for the compact specimen whose limit load failure criterion is approximated by upper and lower bound limit load solutions

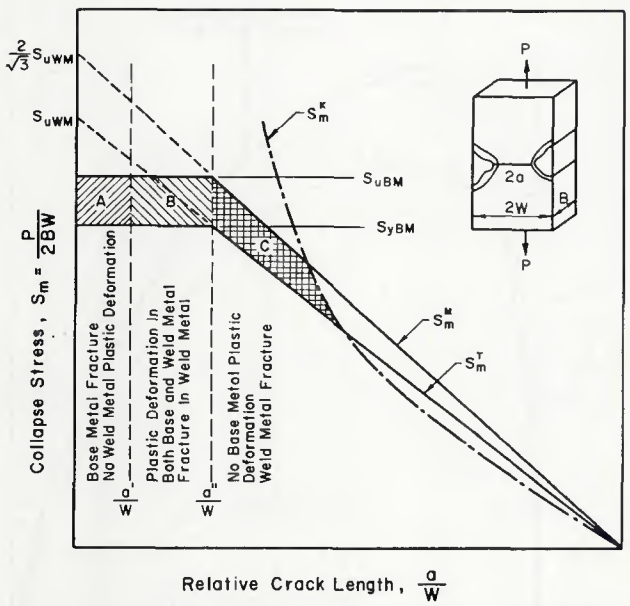

Fig. 5 — Extension of the two failure criteria model to overmatched, high fracture toughness, butt joint weldments containing planar discontinuities

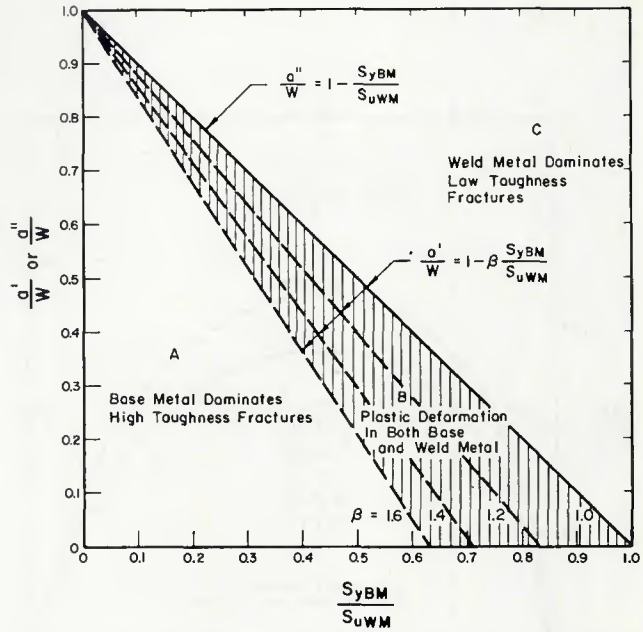

Fig. 6 — The effects of weld metal overmatching and work hardening on the transition flaw widths a′/W and a″/W

where Y is the compliance function for a compact specimen given in the ASTM standard K_{Ic} test method.

The relationship between the two failure criteria for the compact specimen is shown in Fig. 4. Whenever the LL failure criterion predicted a lower collapse load, it dominated the fracture, as shown for the smaller b/W values. Similarly, the fracture will be characterized by the FT failure criterion when it predicts the lower load value; this is indicated for the larger b/W values. The intersection and relative locations of the two failure criteria are dependent on the specimen dimensions and the material's tensile strength and fracture toughness.

Application of the Two Failure Criteria Model to Steel Weldments

The feasibility of applying a two failure criteria model was first established by comparing predicted with actual fracture behavior of more simple wrought steels. Excellent agreement was found between predicted and actual behavior for a wide range in steels, from low strength, plain carbon structural grades to the quenched and tempered hardenable steels. Specific details concerning the predicted and actual fracture behavior of these steels are given in Ref. 22.

Weldments, however, are heterogeneous structural elements composed of at least three microstructural regions: base metal (BM), weld metal (WM), and heat-affected zone (HAZ). Each of these regions has a different yield strength, tensile strength, and fracture toughness. The weld metal usually has a higher tensile and yield strength than the base metal and is said to be "overmatched." Strengths and toughnesses of the HAZ are highly variable depending on the material, but are assumed for discussion purposes to be intermediate to the BM and WM.

Very small flaws in tough, overmatched weld metal ($S_{yWM} > S_{uBM}$) are of minor consequence, since failure will occur in the base metal at loads less than those required for plastic deformation in the weld metal net section. The load carrying capacity of these weldments is thus limited by the tensile strength of the base metal, as illustrated by Region A in Fig. 5. The maximum flaw width (a′/W) that will result in base metal controlled fracture can be estimated by equating the collapse stress predicted by the Tresca value of the LL failure criterion to the base metal tensile strength:

$$S_{uBM} = S_{uWM}\left(1 - \frac{a}{W}\right) \qquad (12)$$

When solved for a′ this equation becomes

$$\frac{a'}{W} = 1 - \frac{S_{uBM}}{S_{uWM}} \qquad (13)$$

Flaw widths greater than a′/W cause both the base and weld metals to plastically deform, but final fracture occurs in the flawed weld metal. Because the lower strength base metal is part of the fracture process, the collapse loads are limited by the base metal tensile strength. The tensile behavior of these flawed weldments is shown as Region B in Fig. 5.

Beyond a certain flaw size (a″/W), fracture occurs in the flawed weld metal at stresses less than the base metal yield strength. Weldments containing these larger flaws fail in the weld metal and exhibit tensile behavior in accordance with the LL failure criterion, as shown by Region C in Fig. 5. The value of a″/W can be estimated by equating the Tresca LL failure criterion to the base metal yield strength:

$$S_{yBM} = S_{uWM}\left(1 - \frac{a}{W}\right) \qquad (14)$$

Solving for a″/W gives the equation:

$$\frac{a''}{W} = 1 - \frac{S_{yBM}}{S_{uWM}} \qquad (15)$$

The relative values of a′/W and a″/W shown in Fig. 5 are dependent on the tensile and yield strength of both the base and weld metals, that is, the degree of overmatching. The curves shown in Fig. 6 illustrate the effect that the degree of overmatching (S_{yBM}/S_{uWM}) has on a′/W and a″/W and how overmatching affects the extent of Regions A, B and C shown in Fig. 5.

The combinations of relative flaw width and overmatching that cause fracture in the base metal prior to yielding of the weld metal net section are contained within Region A. Since the fracture is completely controlled by the unflawed base metal, large amounts of plastic deformation occur, and the stress at fracture is approximately equal to the base metal tensile strength. Region A represents high toughness joints for which weld metal flaws are benign under static loading.

The relative flaw widths and degree of overmatching included in Region B of Fig. 6 result in fractures in which both the base and weld metals deform plastically. The apparent joint toughness is still high because large amounts of plastic work are expended in deforming the base metal. The extent of Region B varies with the amount of work hardening (β) available in both the base and weld metals. The value of β is defined as:

$$\beta = \frac{S_{uBM}}{S_{yBM}} \cdot \frac{S_{uWM}}{S_{yWM}} \qquad (16)$$

The boundary separating Region B from Region A is given by the equation:

$$\frac{a'}{W} = 1 - \beta \frac{S_{yBM}}{S_{uWM}} \qquad (17)$$

and the boundary between Region B and Region C is expressed by:

$$\frac{a''}{W} = 1 - \frac{S_{yBM}}{S_{uWM}} \qquad (18)$$

The extent of Region B, therefore, is dependent on the degree of overmatching and on the work hardening of the base and weld metals. That is, Region B diminishes as the degree of overmatching (S_{yBM}/S_{uWM}) approaches zero or when both the base and weld metal do not work harden ($\beta = 1.0$).

Referring to Fig. 5, the fracture behavior of high toughness weldments (large $K_c/S_u \sqrt{W}$) was divided into three regions separated by the transition flaw widths a′/W and a″/W. A weldment containing weld metal flaw widths less than a″/W will reach a collapse stress (S_m) approximately equal to the base metal tensile strength. Flaw widths greater than a″/W cause a reduction in S_m as predicted by the limit load failure criterion. Fracture toughness controlled failures may occur for very large a/W at stresses predicted by the curve labeled S_m^K as previously discussed.

Table 1—Chemical Compositions of Base Metal and Filler Metal[a]

Element	Base Metal[b] (wt-%)	Filler Metal[c] (wt-%)
C	0.16	0.08
Mn	0.82	1.70
P	0.012	0.005
S	0.019	0.009
Si	0.23	0.46
Cu	0.27	–
Ni	0.76	2.40
Cr	0.54	0.05
Mo	0.47	0.50
V	0.06	0.02
B	0.004	–
Al	–	0.003
Ti	–	0.025

[a]Compositions supplied by manufacturer.
[b]Ladle analysis A514 Grade F (¾-in. plate).
[c]1/16-in. diam. bare wire; 110 ksi Y.S. for GMAW.

Comparison of Predicted Fracture Behavior with Experimental Results

The effect of weld metal discontinuities on the fracture behavior of a structural steel was investigated using ASTM A514 grade F (standard specification for high yield-strength, quenched and tempered alloy steel plate, suitable for welding) base metal welded with ER120S-1 solid wire electrode. Chemical analyses of the base metal and filler metal are given in Table 1. Table 2 gives the tensile and yield strength values of the base metal and for weld metal coupons prepared with four different welding heat inputs. Weldments were fabricated with internal full-length, incomplete joint penetration (IJP) discontinuities, which resulted in the CCT specimen geometry shown in Fig. 7. An enlarged view of the IJP test section is shown in Fig. 8.

The test specimens were welded

Table 2—Small Specimen Tensile Properties

Specimen	Location	Base Metal Properties[a] Sy (ksi)	Su (ksi)
T-1	Longit.	112.5	122.9
T-2	Longit.	108.7	121.6
T-3	Transv.	105.9	122.7
Avg.		109.0	122.4

Specimen	Heat Input (kJ/in.)	Weld Metal Properties[b] Sy (ksi)	Su (ksi)
20-1	20	117.1	136.5
20-2	20	118.1	139.0
Avg.		117.6	137.8
30-1	30	129.1	143.6
30-2	30	125.9	138.7
30-3	30	124.3	138.8
Avg.		126.4	140.2
50-1	50	106.9	132.4
50-2	50	96.7	137.5
Avg.		101.8	135.0
90-1	90	81.5	113.0
90-2	90	83.5	115.1
Avg.		82.5	114.1

[a]Overall specimen length 4.00 in., 1.00-in. gage length, 0.223-in. diam. reduced section.
[b]Overall specimen length 5.00 in., 1.00-in. gage length, 0.250-in. diam. reduced section – except 30 series: 0.314-in. diam. reduced section.

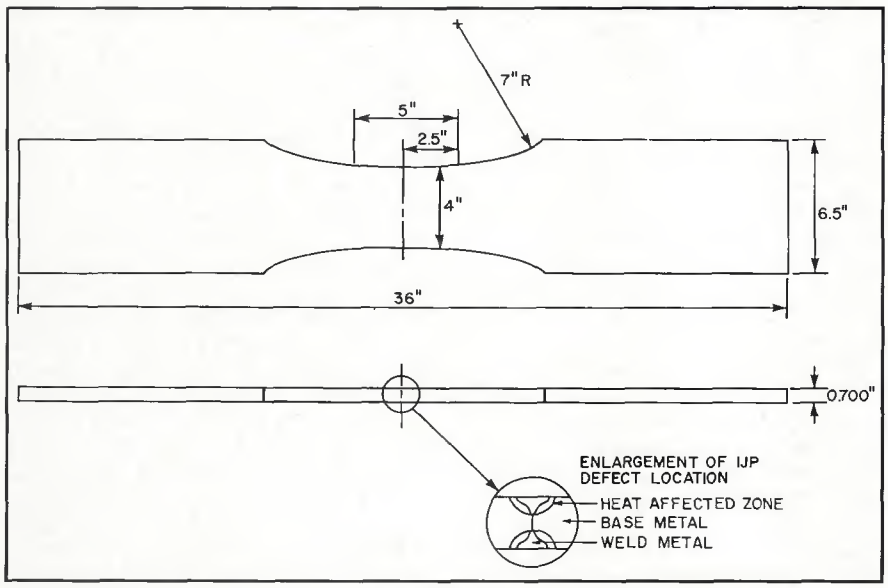

Fig. 7—Dimensions of butt joint welded A514F/ER120S-1 specimens containing incomplete joint penetration discontinuities

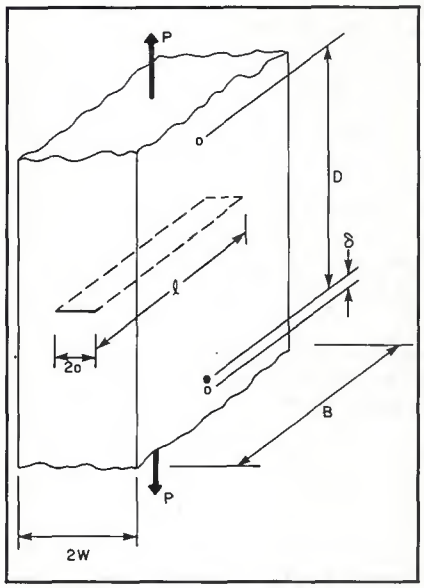

Fig. 8—Enlarged view of the test section shown in Fig. 7

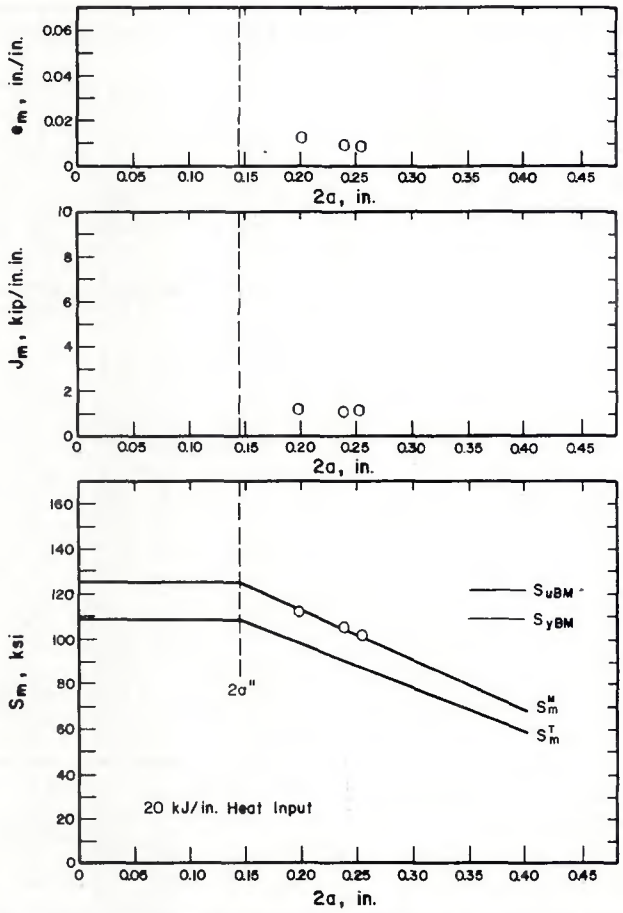

Fig. 9—Experimental results of specimens fabricated with 20-kJ/in. heat input welds. The collapse stress, S_m, data lie within the Tresca (S_m^T) and von Mises (S_m^M) limit load predictions

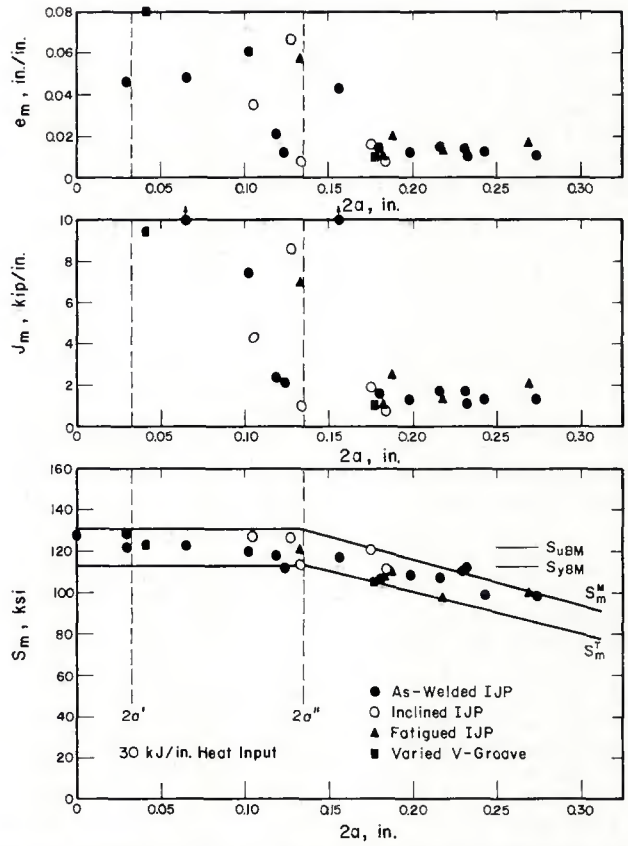

Fig. 10—Experimental results of specimens fabricated with 30-kJ/in. heat input welds. The collapse stress, S_m, data lie within the Tresca (S_m^T) and von Mises (S_m^M) limit load predictions. The strain at maximum load (e_m) and J-integral data show a transition from high to low values at the flaw width, 2a"

together using a 60-deg double V-groove preparation with a variable root face to control the width (2a) of the IJP. The welding variables used to fabricate the specimens are listed in Table 3. The travel speed was varied to produce the desired heat input in the weld metal. Most of the specimens were fabricated with a single 30-kJ/in. (1.2-kJ/mm) weld pass per side. Other specimens were similarly fabricated, except that welding heat inputs of 20, 50 and 90 kJ/in. (0.8, 2, and 3.5 kJ/mm) were used.

Most of the specimens contained full length IJP discontinuities. All specimens were pulled in tension to failure in the as-welded condition. Other specimens were tested after the IJP was fatigue sharpened, and some specimens were fabricated with altered groove angles or inclined IJP's. A complete discussion of the test results obtained from these specimens is given in Ref. 4. In general, altering the IJP discontinuity had little effect on the tensile behavior.

Table 3—Welding Variables Used on Test Specimens

Welding process	Gas Metal Arc (GMA)
Voltage	28–30 V
Current	285–295 A
Preheat and interpass temperature	200°F
Shielding gas composition	98% Ar–2% O_2

Both load and deformation responses were digitally recorded during testing and computer analyzed after testing to determine the weldment yield strength (S_y), collapse stress (S_m), collapse strain (e_m) and the value of J at maximum load (J_m). Values of e_m, J_m and S_m are plotted in Figs. 9–12 for welding heat inputs of 20, 30, 50 and 90 kJ/in., respectively. In these same figures, the S_m data are compared with the collapse stresses predicted by the Tresca and von Mises values of the LL failure criterion (Equations 2 and 3). The transition flaw sizes 2a' and 2a" were determined using Equations 13 and 15.

Since more specimens were welded with a 30 kJ/in. heat input, this group provided the best comparison between the theorized tensile behavior (Fig. 5) and experimental results (Fig. 10). Examining first the e_m data in Fig. 10, it can be seen that e_m reached a lower limiting value at flaw widths greater than 2a". As 2a decreased, e_m increased. A similar response was seen in the J_m data. The lower limiting value of J_m occurred for values of 2a greater than 2a". When the crack width exceeded 2a", all plastic deformation was confined to the uncracked ligaments. Fictitiously high values of J_m were calculated in specimens containing crack widths less than 2a" as a result of base metal plastic deformation not associated with the crack tips being included in the measurements. Collapse stress (S_m) data for the 30-kJ/in. specimens agreed quite well with the tensile behavior predicted by the LL failure criterion. The similar, good agreement with the predicted collapse stress values was also found in the experimental results for the 20-, 50- and 90-kJ/in. heat input specimens shown in Figs. 9, 11 and 12. With the exception of one 50-kJ/in. specimen, which contained secondary discontinuities, all the experimental S_m values

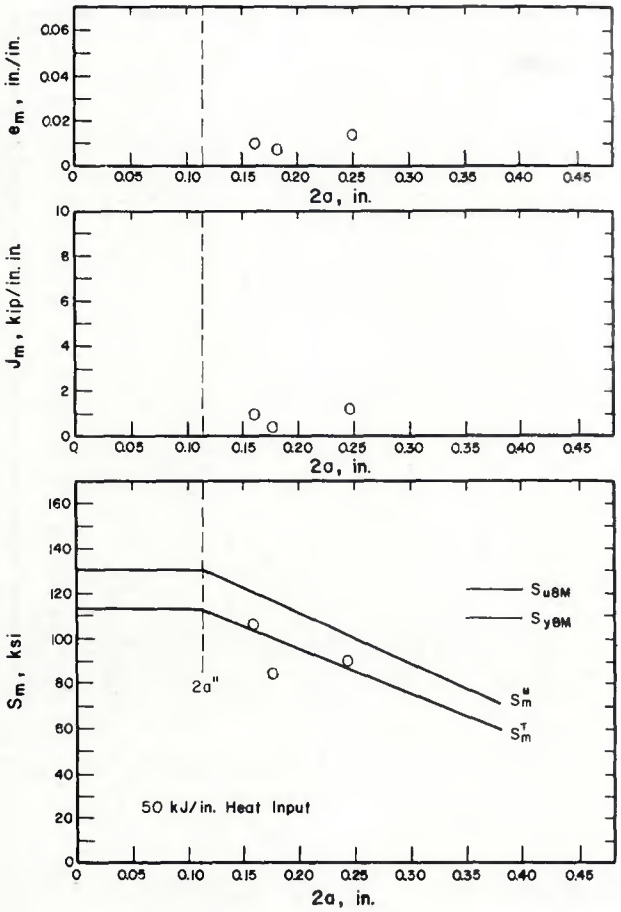

Fig. 11—Experimental results of specimens fabricated with 50-kJ/in. heat input welds. The low e_m, J_m and S_m data points resulted from a specimen containing secondary discontinuities

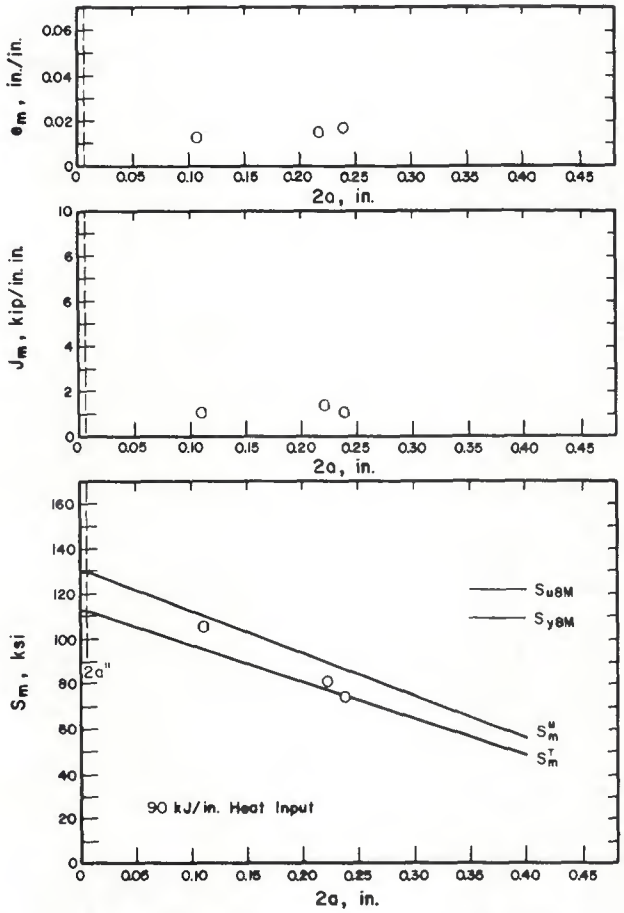

Fig. 12—Experimental results of specimens fabricated with 90-kJ/in. heat input welds. Note that the limit load failure criterion controls the fracture behavior over almost the entire range of 2a

were within the range predicted by the Tresca and von Mises values of the LL failure criterion.

Values of the J-integral fracture toughness varied for each of the welding heat inputs evaluated. Average valid J_m values measured for each heat input are given in Table 4.

For the CCT specimen having the dimensions shown in Fig. 7, the weld metal values of $K_c/S_u\sqrt{W}$ ranged from 2.29 to 2.74. Referring to Fig. 2, it can be seen that all the test specimens were well within the region where the limit load failure criterion dominated the fracture behavior.[1]

The calculated value of 2a′ (base metal dominated fracture) for the 30-kJ/in. heat input welds was 0.032 in. (0.8 mm). This was the only 2a′ that could be calculated because the S_{yWM} values for the other heat inputs were all less than S_{uBM}. Consequently, only the 30-kJ/in. heat input specimens exhibited tensile behavior corresponding to Region A in Fig. 5, *i.e.*, failure completely controlled by base metal mechanical properties.

Values of 2a″ (the minimum flaw width corresponding to limit load controlled fracture in the weld metal) were calculated for each weldment—Table 5. The 2a″ values, which are shown in Figs. 9–12, were calculated using Equation 15.

The 2a″ transition flaw width decreased as the degree of overmatching decreased. The calculated 2a″ value for the 90-kJ/in. heat input specimens (Fig. 12) was 0.007 in. (0.2 mm), which meant that the tensile behavior was controlled by the limit load failure criterion for nearly all flaw widths. Only flaw widths less than approximately 0.007 in. would cause the base metal to participate in the fracture process; otherwise, fracture is completely controlled by the weld metal net section.

The J-integral derived fracture toughness values could not be used to accurately predict the collapse stress values of the weld specimens using LEFM equations. Even enlarging the effective crack

Table 4—Averages of Maximum Load for Each Heat Input

Heat Input (kJ/in.)	Average Valid J_m Value (ksi)
20	1.17
30	1.43
50	1.15
90	1.14

Table 5—Minimum Flaw Width in Weld Metal

Heat Input	S_{yBM}/S_uWM	2a″
20	0.79	0.146 in.
30	0.81	0.135
50	0.84	0.114
90	0.99	0.007

(1)The weld metal $K_c/S_u\sqrt{W}$ values ranging from 2.29 to 2.74 were measured experimentally and are correct for the ASTM A514F steel weldments. The 2.29 to 2.74 range in $K_c/S_u\sqrt{W}$ is above the arbitrary cutoff for the vertical scale of Fig. 2, but nevertheless, is well outside the region shown for FT controlled failure. The reader will note that there is no discrepancy, in that the data points are simply outside the scale for Fig. 2.

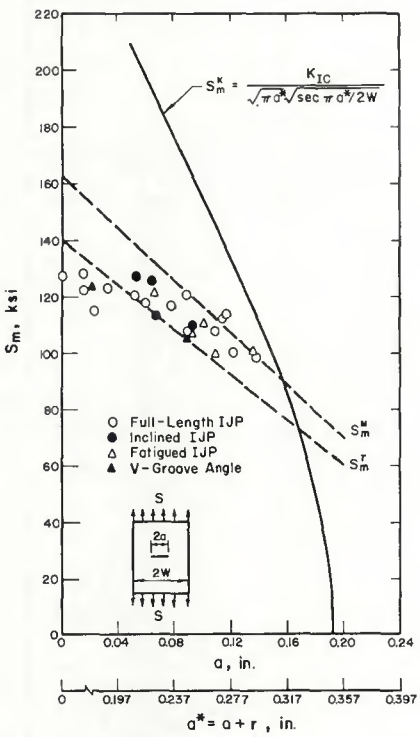

Fig. 13 — Comparison of A514F/ER120S-1 flawed weldment data with collapse stresses predicted by the limit load and fracture toughness failure criteria. The S_m^K curve was corrected for the crack tip plastic zone (r)

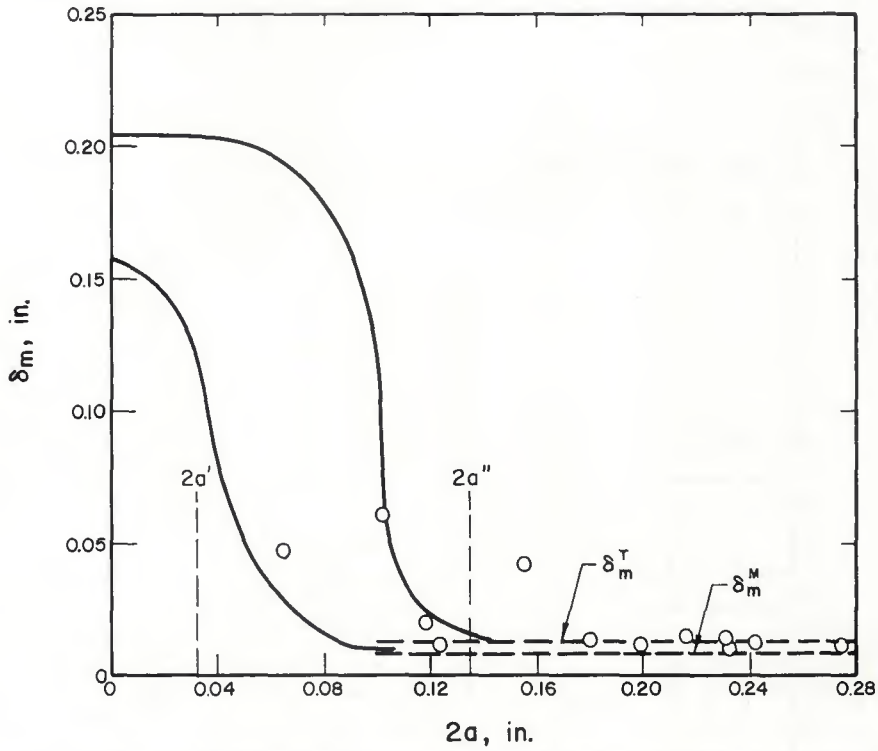

Fig. 15 — Comparison of the deformation at maximum load (δ_m) data with the values predicted for as-welded, 30-kJ/in. heat input weldments

size by applying the plastic zone correction still rendered the predicted collapse stress values unconservative, as shown in Fig. 13. Such unconservative collapse stress values, due to an apparent misuse of fracture mechanics, are potentially dangerous when structural reliability is based on calculations of this kind. Fracture toughness values are useful, however, provided the plastic deformation is confined to the uncracked ligaments adjacent to the crack tips (Region C in Fig. 6). Under such conditions, the tensile behavior can be approximated by a rigid plastic load-deflection curve — Fig. 14. With the maximum stress bounded by the LL failure criterion, the work extracted during fracture is confined to the plastic deformation of the uncracked ligaments, *i.e.*, the J-integral value of fracture toughness. Working backward from this premise, once the flaw size, LL collapse stress, and J-integral toughness are known, the deformation at maximum (δ_m) load can be calculated as follows:

$$\delta_m = \frac{J_m}{S_m}\left[1 - \frac{a}{W}\right] \qquad (19)$$

As shown in Fig. 15, the agreement between predicted and measured values is good for IJP widths greater than 2a".

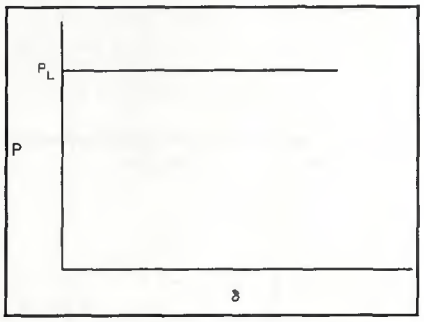

Fig. 14 — Load versus deflection for a rigid-plastic material

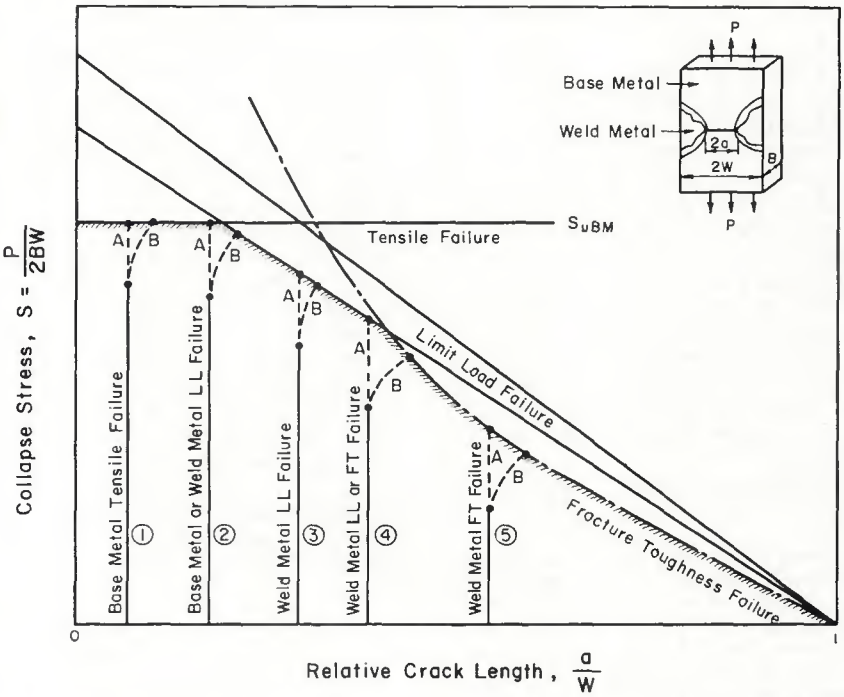

Fig. 16 — The effects of subcritical crack extension on the two failure criteria model for a centrally flawed butt joint weldment. For a given initial crack length, specimens not undergoing subcritical crack extension follow Trajectory A, while those that exhibit subcritical crack extension will follow a trajectory such as B

Poor agreement for smaller IJP widths was attributed to gross section plasticity of the material outside the uncracked ligaments. Nevertheless, the deformation at maximum load values were conservative and suitable for engineering applications.

The Effect of Subcritical Crack Extension

The two failure criteria model was shown to predict the collapse loads of flawed structural materials, to determine *a priori* whether the fracture behavior would be predominantly elastic or elastic-plastic, and to establish the deformation at collapse. The model thus far presented was based on two major assumptions: (1) fracture toughness failures are characterized by LEFM with negligible plastic deformation, and (2) no subcritical crack extension occurred prior to failure.

Subcritical crack extension, however, has been shown to significantly affect the critical value of the J-integral (Ref. 23). In the same study, J-integral crack-extension resistance (R) curves were observed to be geometry and section size dependent. Hence, subcritical crack extension is believed to affect the two criteria fracture model by altering the load-crack length trajectory prior to collapse. This effect is schematically illustrated for an overmatched butt joint weld containing a centralized, planar discontinuity in Fig. 16. Trajectory A represents the stress-crack length trajectory for an IJP flaw which does not undergo subcritical crack extension; fracture occurs by the failure criterion that Trajectory A encounters first. If the material exhibits subcritical crack extension, then its stress-crack length trajectory may follow a trajectory similar to those illustrated by the B curves.

The onset of subcritical crack growth occurs when the value of J at the crack tip exceeds the value of J_{Ic} (Ref. 23). The trajectory from this point until fracture occurs is dependent on the tearing behavior of the material. Final fracture occurs when the stress-crack length trajectory intersects one of the failure criteria. As seen in Curves 2 and 4 in Fig. 16, the occurrence of subcritical crack extension can change the controlling failure criterion and, to some extent, the collapse load.

The stable tearing behavior of structural materials has been described by Paris, *et al.* (Ref. 24), in terms of a tearing modulus (T)—Fig. 17. Initial crack extension is attributed to crack tip blunting in proportion to the instantaneous value of J:

$$\Delta a \approx \frac{1}{2}\frac{J}{S_o} \qquad (20)$$

where: S_o = the tensile flow stress.

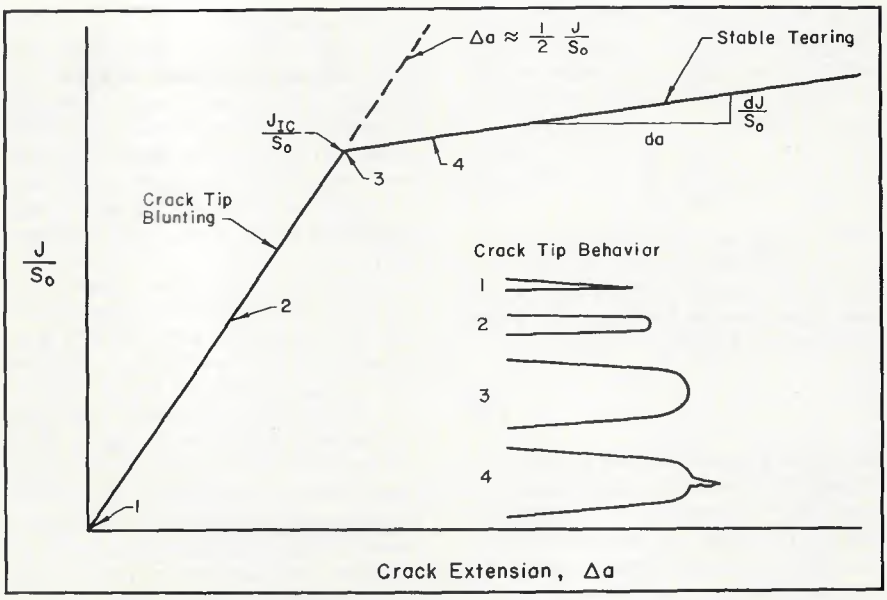

Fig. 17 — J-integral R-curve illustrating the crack tip behavior as J increases. The crack tip blunts in the region $0 < J/S_o < J_{Ic}/S_o$, followed by stable crack extension by tearing when $J/S_o > J_{Ic}/S_o$

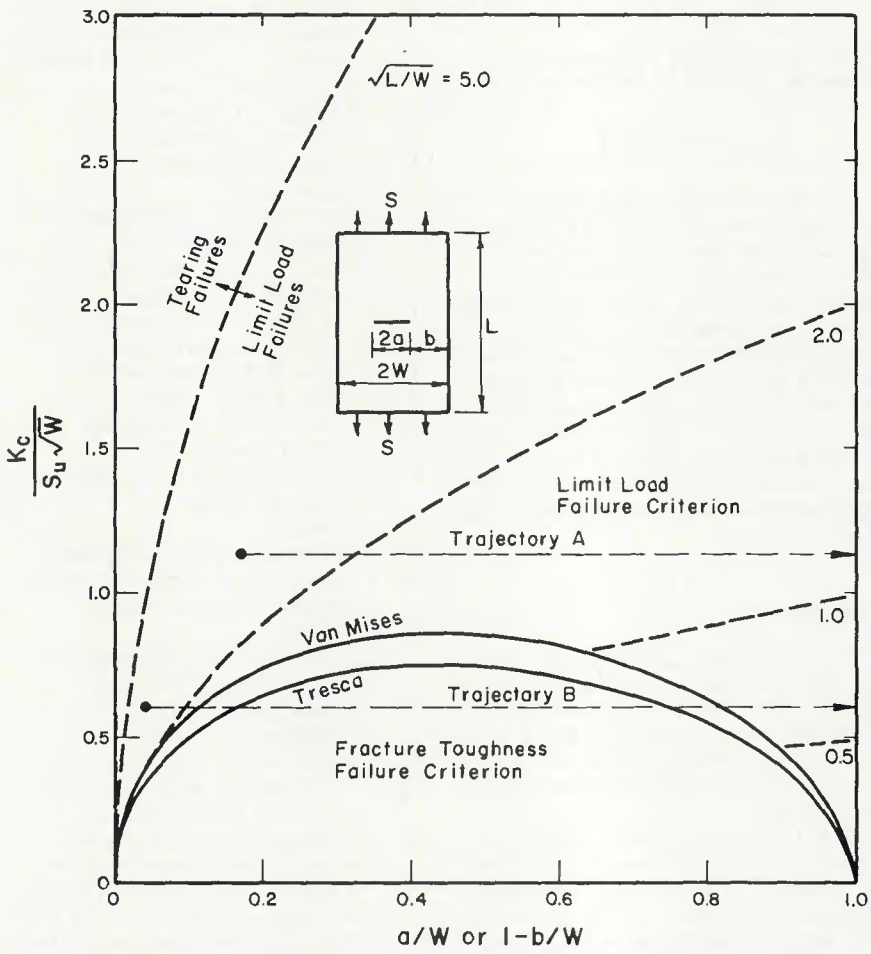

Fig. 18 — The effects of stable tearing on the fracture behavior of center-crack tension specimens. Subcritical crack extension may occur at a constant value of $K_c/S_u\sqrt{W}$ until either the limit load or fracture toughness failure criterion controlled region is encountered

When the applied J reaches J_{Ic}, crack extension by "stable tearing" commences. The slope of the stable tearing portion of the curve determines the value of T; that is:

$$T = \frac{dJ}{da} \cdot \frac{E}{S_o^2} \tag{21}$$

The effect of stable tearing can be incorporated into the two failure criteria model for a center-crack tension specimen, since unstable limit load failure was stated to occur (Ref. 24) whenever:

$$T \leq \frac{L}{W} \tag{22}$$

The critical K values determined from the J-integral tests on CCT welded specimens have been denoted K_c to distinguish these values from the ASTM E399 fracture toughness K_{Ic}, hence all K_c values are J derived; that is:

$$K_c^2 = J_{Ic}E \tag{23}$$

Substituting Equation 23 into Equation 21 and combining this with Equation 22 results in:

$$T \approx \frac{d\,(K^2)}{da} \cdot \frac{1}{S_o^2} \leq \frac{L}{W} \tag{24}$$

When Equation 24 is integrated and subsequently divided by $\sqrt{W}$ the result is:

$$\frac{K}{S_o\sqrt{W}} \leq [\frac{L}{W} \cdot \frac{a}{W}]^{1/2} \tag{25}$$

Curves determined from Equation 25 for various values of $\sqrt{L/W}$ are shown in Fig. 18 for the center-crack tension specimen. Subcritical crack extension precedes final fracture in the region lying above the appropriate $\sqrt{L/W}$ line, and below this line no subcritical crack extension will occur prior to fracture. Bodies prone to subcritical crack extension follow a $K_c/S_u\sqrt{W} - a/W$ trajectory (horizontal lines in Fig. 18) until one of the failure criteria is encountered or until the crack progresses completely through the cross-section.

Conclusions

1. The collapse stresses of high-strength structural steel weldments containing incomplete joint penetration discontinuities were predicted by a two failure criteria model, based on plastic limit load theory and linear elastic fracture mechanics.

2. For a given geometry and crack length, the fracture behavior was shown to depend on the fracture toughness, strength and section size of the body. Fracture governed by the fracture toughness failure criterion occurred for low values of $K_c/S_u\sqrt{W}$, and limit load controlled fractures occurred for larger $K_c/S_u\sqrt{W}$ values.

3. Weldments fabricated from high $K_c/S_u\sqrt{W}$ materials failed at loads predicted by the limit load failure criterion at incomplete joint penetration widths greater than 2a″. The degree of weld metal overmatching was shown to control the value of 2a″ that separated high toughness joints from low toughness joints.

4. The deformation at collapse was predicted from J-integral fracture toughness measurements and the limit load failure criterion for weldments containing flaw widths greater than 2a″.

5. Subcritical crack extension by a stable tearing phenomenon had a small effect on the two failure criterion model. Crack extension may change the controlling failure criterion, thereby resulting in a lower collapse stress; or in some instances, the entire fracture process may be controlled by stable tearing.

Appendix

List of Symbols

a	Crack width or length
a'	Maximum crack width for base metal controlled fracture
a''	Minimum flaw width for yielding in weld.metal only
Δa	Change in crack length
B	Specimen thickness
b	Uncracked ligament
D	Gage length
d	Span distance of bend specimen
E	Young's modulus
e_m	Strain at maximum load
J	Value of the J-integral
J_{Ic}	Value of J at the onset of crack extension in plane strain
J_m	Value of J at maximum load
K	Stress intensity factor
K_c	Critical value of the stress intensity factor
K_{Ic}	Critical value of K_c in plane strain
L	Specimen length
P	Specimen load
P_m	Maximum load (collapse load)
P_K	Collapse stress predicted by the fracture toughness failure criterion
P_L	Collapse stress predicted by the limit load failure criterion
r	Crack length plastic zone adjustment factor
S	Gross section stress
S_m	Gross section collapse stress (at maximum load)
S_m^K	Collapse stress predicted by linear elastic fracture mechanics
S_m^M	Collapse stress predicted by the von Mises value of the limit load
S_m^T	Collapse stress predicted by the Tresca value of the limit load failure criterion
S_o	Tensile flow stress
S_y	Uniaxial yield strength
S_{yBM}	Base metal yield strength
S_{yWM}	Weld metal yield strength
S_u	Uniaxial tensile strength (ultimate strength)
S_{uBM}	Base metal tensile strength
S_{uWM}	Weld metal tensile strength
T	Tearing modulus
W	Specimen width
Y	Compliance function $-F(a/W)$
β	Work hardening factor for weldments
δ	Deformation in gage length
δ_m	Deformation at maximum load (collapse)
τ	Shear stress
τ_o	Shear flow stress

References

1. Lawrence, F. V., Jr., Radziminski, J. B., and Kruzic, R. W. Oct. 1971. *The Effect of Porosity on the Static Tensile Strength of High-Strength Structural Steel Weldments.* Report to U.S. Army Corps of Engineers, Construction Engineering Research Laboratory, Champaign, Ill.

2. Lawrence, F. V., Jr., and Cox, E. P. Jan. 1974. *The Effect of Lack of Penetration Defects on the Static Tensile Behavior of High-Strength Structural Steel Weldments.* Report to U.S. Army Corps of Engineers, Construction Engineering Research Laboratory, Champaign, Ill.

3. Lawrence, F. V., Jr., and Cox, E. P. June 1974. *The Influence of Heat Input and Lack of Penetration Length on the Static Tensile Strength of High-Strength Structural Steel Weldments.* Report to U.S. Army Corps of Engineers, Construction Engineering Research Laboratory, Champaign, Ill.

4. Lawrence, F. V., Jr., and Cox, E. P. 1976. Influence of inadequate joint penetration on tensile behavior of A514 steel welds. *Welding Journal* 55(5):113-s to 120-s.

5. Cox, E. P., and Lamba, H. S. 1984. Cluster porosity effects on transverse fillet weld strength. *Welding Journal* 63(1):1-s to 7-s.

6. Lundin, C. D. Dec. 1976. The significance of weld discontinuities—a review of current literature. *WRC Bull. 222.*

7. Lundin, C. D. June 1984. Fundamentals of weld discontinuities and their significance. *WRC Bull. 295.*

8. Rice, J. R. 1968. A path independent integral and the approximate analysis of strain concentration by notches and cracks. *Journal of Applied Mechanics* 35:379–386.

9. Begley, J. A., and Landes, J. D. 1972. The J-integral as a fracture criterion. *Fracture Toughness, Proc., 1971 National Symposium on Fracture Mechanics, Part II.* ASTM, Special Technical Publications 514, pp. 1–23.

10. Landes, J. D., and Begley, J. A. 1972. The effect of specimen geometry on J_{Ic}. *Fracture Toughness, Proc., 1971 National Symposium on Fracture Mechanics, Part II.* Ibid, pp. 24–39.

11. Lawrence, F. V., Jr., and Cox, E. P. Sept. 1973. *The Effect of Lack of Penetration Defects on the Static Tensile Behavior of High-Strength Structural Steel Weldments.* Technical Report UILU-ENG-73-2011; also, Construction Engineering Research Laboratory

Technical Report M-123, Champaign, Ill., 1975.

12. Lawrence, F. V., Jr., and Cox, E. P. 1975. *Influence of Heat Input and Lack of Penetration Length on Static Tensile Strength of High-Strength Structural Steel Weldments.* Construction Engineering Research Laboratory Technical Report M-135, Champaign, Ill.

13. Cox, E. P. Unpublished research.

14. Dowling, A. R., and Townley, C. H. A. 1975. The effect of defects on structural failure: a two-criteria approach. *International Journal of Pressure Vessels and Piping* 3:2-31.

15. Drucker, D. C., Prager, W., and Greenberg, H. J. 1952. Extended limit design theorems for continuous media. *Quarterly of Applied Mathematics* 9:381-389.

16. Drucker, D. C. 1968. Macroscopic fundamentals in brittle fracture. *Fracture,* H. Liebowitz, Ed., Vol. 1, Academic Press, New York, N.Y., pp. 474-529.

17. McClintock, F. A. 1961. On notch sensitivity. *Welding Journal* 40(5):202-s to 208-s.

18. Standard method of test for plane-strain fracture toughness of metallic materials. Part 10, E399, *1981 Annual Book of ASTM Standards.*

19. Standard method of determining J_{Ic}—a measure of fracture toughness. Part 10, E813, *1981 Annual Book of ASTM Standards.*

20. Rice, J. R. 1972. The line spring model for surface flaws. *The Surface Crack: Physical Problems and Computational Solutions.* American Society of Mechanical Engineers, New York, N. Y., pp. 171-185.

21. Ewing, D. J. E., and Richards, L. E. 1974. The yield-point loads of singly-notched pin-loaded tensile strips. *Journal of the Mechanics and Physics of Solids* 22:27-36.

22. Cox, E. P., and Lawrence, F. V., Jr. 1980. Ductile fracture behavior of wrought steels. *Fracture Mechanics: Twelfth Conference,* ASTM STP 700, American Society for Testing and Materials, pp. 529-551.

23. Landes, J. D., and Begley, J. A. 1974. Test results from J-integral studies: an attempt to establish a J_{Ic} testing procedure. *Fracture Analysis,* ASTM, Special Technical Publication 560, pp. 170-186.

24. Paris, P. C., Tada, H., Zahoor, A., and Ernst, H. 1977. *A Treatment of the Subject of Tearing Instability.* NUREG-0311, U.S. Nuclear Regulatory Commission, Aug. 1977; see also *Elastic-Plastic Fracture,* ASTM STP 668, American Society for Testing and Materials, 1979, pp. 5-36.

WRC Bulletin 317
August 1986

PVRC Centrifugal Pump-Piping Interaction Experience Survey
By J. R. Payne

Over 100 questionnaires asking about field experience, design standards, and attitudes on the effect of pipe reactions on centrifugal pumps were received from the power and process industries. This survey, which was prompted by industry inquiries, examines the experience and needs of piping and pump system designers, manufacturers, and operators. It was designed to help the Pressure Vessel Research Committee (PVRC) determine whether a significant pump-piping interaction problem exists and to what extent, and also to help set research priorities and provide guidance to code and standards bodies.

The survey and publication of this report was sponsored by the Subcommittee on Piping, Pumps and Valves of the Pressure Vessel Research Committee of the Welding Research Council. The price of WRC Bulletin 317 is $22.00 per copy, plus $5.00 for postage and handling. Orders should be sent with payment to the Welding Research Council, Suite 1301, 345 E. 47th St., New York, NY 10017.

WRC Bulletin 318
September 1986

The primary objective of this Bulletin, which contains two papers, is to present a comprehensive picture of the research work conducted to establish the current techniques and procedures for specifying the ferrite content of austenitic stainless steel weld metal and measuring its level.

Factors Influencing the Measurement of Ferrite Content in Austenitic Stainless Steel Weld Metal Using Magnetic Instruments
By E. W. Pickering, E. S. Robitz and D. M. Vandergriff

This report describes a program conducted under the auspices of the Welding Research Council (WRC) Subcommittee on Welding Stainless Steel to identify the optimum procedure for the preparation of austenitic stainless steel weld samples for Ferrite Number (FN) determination.

Measurement of Ferrite Content in Austenitic Stainless Steel Weld Metal Giving Internationally Reproducible Results
By E. Stalmasek

This report is a summary of the results of 14 years' work by the IIW Commission 2 in the field of ferrite content measurement, done prior to 1978.

The publication of these reports was sponsored by the Subcommittee on Welding Stainless Steel of the High Alloys Committee of the Welding Research Council. The price of WRC Bulletin 318 is $24.00 per copy, plus $5.00 for postage and handling. Orders should be sent with payment to the Welding Research Council, Suite 1301, 345 E. 47th St., New York, NY 10017.